General Disclaimer

One or more of the Following Statements may affect this Document

- This document has been reproduced from the best copy furnished by the organizational source. It is being released in the interest of making available as much information as possible.

- This document may contain data, which exceeds the sheet parameters. It was furnished in this condition by the organizational source and is the best copy available.

- This document may contain tone-on-tone or color graphs, charts and/or pictures, which have been reproduced in black and white.

- This document is paginated as submitted by the original source.

- Portions of this document are not fully legible due to the historical nature of some of the material. However, it is the best reproduction available from the original submission.

Produced by the NASA Center for Aerospace Information (CASI)

Photon scattering cross sections of H_2 and He

measured with synchrotron radiation*

Gene E. Ice, Mau Hsiung Chen, and Bernd Crasemann

Department of Physics, University of Oregon

Eugene, Oregon 97403

Total (elastic + inelastic) differential photon scattering cross sections have been measured for H_2 gas over a range of $2.5 \leqslant S = (4\pi/\lambda) \sin(\theta/2) \leqslant 6.7$ Å^{-1} and for He over $3 \leqslant S \leqslant 11.2$ Å^{-1}, using an x-ray beam in the Stanford Synchrotron Radiation Laboratory. Absolute measured cross sections agree with theory within the probable errors. Relative cross sections (normalized to theory at large S) agree to better than one percent with theoretical values calculated from wave functions that include the effect of electron-electron Coulomb correlation, but the data deviate significantly from theoretical independent-particle (e.g., Hartree-Fock) results. The ratios of measured absolute He cross sections to those of H_2, at any given S, also agree to better than one percent with theoretical He-to-H_2 cross-section ratios computed from correlated wave functions. It appears that photon scattering constitutes a very promising tool for probing electron correlation in light atoms and molecules. The degree of polarization of the synchrotron radiation beam has been measured by rotating the scattering plane about the beam axis; results are compared with theory.

I. INTRODUCTION

Photon scattering can convey information on the scatterer as well
as on the scattering mechanism. For all but the lightest target atoms,
elastic scattering dominates in the x-ray energy range[1] (Fig. 1); the
corresponding form factor is a transform of the radial charge distribution
about the nucleus, $\rho(r)$. The lightest atoms and molecules are in a
special class: for them, inelastic scattering plays a significant role
in the interaction with photons of x-ray energy. The total (elastic
+ inelastic) scattering cross section then is sensitive to the two-electron
expectation value,

$$P(r) = 4\pi r^2 \sum_{i,j\neq i} \rho_{ij}(r),$$

(1)

where $\rho_{ij}(r)$ is the mean density of electron i with respect to electron j.[2]
Following the Waller-Hartree theory,[3] total differential cross sections as
a function of $S=(4\pi/\lambda)\sin(\theta/2)$ can be inverted to yield the electron-electron
distribution function $P(r)$.[4] The two-electron expectation $P(r)$ is strongly
influenced by electron-electron Coulomb correlation in light atoms, hence
experimental total scattering cross sections can be used to explore the
difference between independent-particle (e.g., Hartree-Fock) and correlated
wave functions. Such a study is reported here.

Good cross sections for the interaction of photons with H_2 and He
are also required in astrophysical work, in order to reconstruct the energy
spectra emitted by stellar sources and to deduce average densities of these
substances in interstellar space.[5,6]

The x-ray scattering cross sections for Z = 1, 2 are so small ($\sim 10^{-24}$ cm^2/atom), that measurements with conventional means are almost impossible.[7,8] The only published work on the subject is that of Wollan,[7] who performed relative measurements limited by the technology of the time. Uncertainties in these results make comparison with theory difficult[9-11] (Fig. 2).

Synchrotron radiation from high-energy electron storage rings now provides an intense source of near-monochromatic, polarized photons with which scattering cross sections can be measured quite accurately, as described here.

II. EXPERIMENT

A. Apparatus

1. Photon source. The experiment was conducted in the Stanford Synchrotron Radiation Laboratory (SSRL),[12] utilizing radiation from electrons that circulate in the Stanford Positron-Electron Accelerator Ring (SPEAR). When the electron energy in the ring is ~ 3 GeV, the synchrotron radiation spectrum peaks near 2 keV and contains substantial intensity up to ~ 15 keV. The photons are emitted in the plane of the circulating electron beam, and tangent to it, within a half angle $\sim mc^2/E_e$. The beam line ("EXAFS 1") used in the present experiment is isolated from the accelerator vacuum by two 0.025-cm thick Be windows and is filled with He to reduce absorption. The photon beam is collimated vertically by a 1-mm slit located 20 m from the circulating electron beam. A nearly monochromatic band of photons ($\Delta E \approx 1$ eV) is selected by Bragg reflection off the 220 planes of a computer-controlled

channel-cut SiO_2 crystal[13](Fig. 3). The photon beam is displaced vertically by the monochromator, but stays parallel to the incident beam. Different Bragg planes can lead to spurious reflections with other energies. In general, these reflections are not in the same plane as the main Bragg reflection, and can be removed by a second collimating slit. The monochromatized photon beam passes through a transmission ion chamber filled with N_2, used to monitor the flux. The beam then enters a heavy interlocked enclosure ("hutch"), in which the scattering chamber is placed. Characteristics of this photon beam which make it particularly attractive for x-ray experiments have been described by Winick and Lindau.[14]

2. Scattering chamber. The sample gas was contained in a stainless-steel scattering chamber[15] illustrated in Fig. 4. Photons scattered into large, well-defined solid angles centered at nominally 60, 90, and 135 deg with respect to the incident beam emerged through 0.013-cm thick Be windows. These windows were machined in a convex shape to permit operation at high pressure (up to 10 atm.) Beam entrance and exit windows were made of flat 0.013-cm thick Be. All Be windows were sealed with In gaskets. Scattered radiation from the entrance and exit windows was suppressed by Al baffles. Circular apertures in the scattering ports defined the solid angle subtended by the detector. The chamber was supported in a cradle which allowed it to be rotated about the beam axis.

3. Photon detection. Scattered x rays were detected with a proportional counter (Reuter-Stokes RSF-G1-M1) filled with 97% Xe and 3% CO_2. The curved Be counter window was 0.013-cm thick by 2.5-cm dia. The x-ray path length in the counter was ~5 cm. Pulses from the counter were processed as indicated

in Fig. 5. The counter was operated at a potential of 1900 V. The signal-to-noise ratio was optimized by placing the FET preamplifier directly next to the counter and insulating both from the metal hutch. A typical spectrum of scattered photons is shown in Fig. 6.

4. Flux monitor. The incident-beam intensity was continually monitored by a N_2-filled transmission ion chamber (Fig. 3). The current from the parallel-plate ion chamber was measured by a Keithley 427 electrometer; the output voltage of the electrometer was converted to frequency and the resultant pulses were counted over one-second sample periods, determined by a Canberra actuator that was controlled by a PDP-11 computer (Fig. 5). The number of counts accumulated during the one-second intervals was added in the computer. To insure that possible fluctuations in the ion-chamber sampling period did not affect results, the proportional-counter output was gated by the same actuator used for the ion chamber.

B. Procedure

1. Alignment. Reproducible placement of the chamber was assured by alignment pins. The vertical placement of the chamber was adjusted by metal shims, to correspond to the beam position at various energies. Accurate positioning of the trimmed photon beam along the center line of the scattering-chamber baffles was verified by placing wires across the chamber windows and exposing Type 57 Polaroid film. This procedure was repeated after each change in azimuthal chamber orientation or in beam energy.

2. Sample gas handling. Very high purity of the sample gases had to be maintained because their cross sections are much lower than those of most

possible contaminants. Helium measurements were made on Matheson UHP
Grade He with a minimum stated purity of 99.9999 percent. The scattering
chamber was flushed with technical grade He for 24 h, then with UHP He for
3-4 h, using a mass-spectrometer leak-tested gas manifold (Fig. 7). Gradual
He flow was maintained during measurements to guard against contamination
by outgassing.

For H_2 measurements, the scattering chamber was pre-flushed with He,
then flushed rapidly for 2-3 h with Matheson UHP H_2 (stated minimum purity
99.999%). A hot Pd-Ag diffusion purifier was then switched into the gas
line. Throughout the measurements, ~1 cm^3/sec of diffusion-purified H_2
was caused to flow through the chamber. It has been determined [16] that
Pd-Ag diffusion purification reduces impurities in H_2 to less than a few
parts in 10^{10}. Measurements repeated after ~24 h during a run gave similar
results, indicating that no gradual changes in gas purity were taking place.

3. Determination of incident-beam energy. The angular position of
the channel-cut monochromator crystal (Fig. 3) is controlled by a stepping
motor that is interfaced for access through a PDP-11 computer. The stepping
motor covers 12.5 deg of crystal rotation in 100,000 steps or "units." At
the beginning of a run, the inflection point in the Cu K absorption edge
(Fig. 8) was conventionally set at 120,000 units. The incident photon energy
E (in eV) is then given in terms of stepping-motor units A by the expression

$$E = 3228.55 \{\sin[(A+48589)/8000]\}^{-1}.$$

(2)

To confirm the calibration, a second absorption edge was mapped out and
its position verified by comparison with tabulated binding energies.

The energy width of the monochromatized synchrotron radiation beam is <10 eV. The width can be estimated from Bragg's law as

$$\Delta E/E = (\cot \theta)\, \Delta\theta, \tag{3}$$

where θ is the Bragg angle and $\Delta\theta$ is the angular divergence of the beam ($\sim 4\times 10^{-5}$ rad). This estimate agrees to 10% with the resolution observed[13] in Br_2 absorption spectra, viz., 2.7 eV at 13.5 keV.

4. _Relative scattering measurements_. Determinations of relative scattering cross sections as a function of $S = (4\pi/\lambda)\sin(\theta/2)$ were performed with high incident x-ray intensity of 10^8 to 10^9 photons per second, available at storage-ring electron energies near 3 GeV. The current from the (upstream) transmission ion chamber was digitalized and placed in the PDP-11 computer memory. The proportional counter detecting scattered photons was gated simultaneously by the computer; counter pulses were stored in the memory of a TRIDAC multiparameter multichannel analyzer. In a 10^3-sec run, $\sim 10^4$ to 10^5 scattered photons could be detected (Fig. 6). A suitable range of "momentum transfer" S could be covered by performing measurements with 5-, 6-, and 7-keV incident photons, scattered through θ=60, 90, and 135 deg. For a given incident photon energy and scattering angle θ, the scattered intensity was measured at three "azimuthal" angles ϕ with respect to the plane of the stored-electron orbit, in which most synchrotron radiation photons are polarized (Sec. III.A). In a few instances, shielding obstructions restricted the number of accessible values of ϕ to two.

The spectra of scattered photons were fitted by least squares to Gaussian peaks with a quadratic background.

5. <u>Absolute measurements and ion-chamber calibration</u>. For absolute measurements of scattering cross sections, the incident x-ray intensity and number of scattered photons were measured in the same manner as described in Sec. II.B.4. The incident flux, however, was kept low ($\sim 10^6$ photons per second), corresponding to storage-ring electron energies near 2 GeV. With this low flux, several hours were required to accumulate $\sim 10^4$ scattered photons. It was then, however, possible to determine the incident flux absolutely. For this purpose, a Pb foil with a fine pinhole was inserted upstream of the transmission ion chamber, allowing but a small fraction of the incident beam to pass and reducing the ion-chamber current proportionately. The reduced x-ray beam could then be attenuated by means of carefully calibrated absorber foils, and the photons in the attenuated beam could be counted directly by means of a Xe-filled proportional counter. The size of the pinhole was so chosen that the ion-chamber current, while small, remained above random fluctuations; in each case, measurements were repeated with pinholes of various diameters. The absorber foils were calibrated by the method of Chipman,[17] using monochromatized x rays from a conventional generator.[8] Suitable corrections for attenuation in air and windows and for dead-time loss were made. The incident-beam intensity had to be kept as low as indicated above because otherwise higher-energy harmonics in the spectrum of the attenuated beam would overlap the n=1 peak. The absolute flux determination was the most difficult part of the experiment, but results obtained by the indicated method were remarkably consistent.

III. RESULTS

A. Beam Polarization

In order to derive the physically significant dependence of the scattering cross sections on the "momentum transfer variable" $S = (4\pi/\lambda)\sin(\theta/2)$, it was necessary to account for the dependence of the scattered intensity on the polarization of the incident photons. If the incident x rays are linearly polarized in a direction that makes an angle ϕ with the scattering plane, then the cross section for scattering through an angle θ depends on ϕ as $1-\sin^2\theta\cos^2\phi$. We consider the incoherent incident beam to be composed of two orthogonal linearly polarized components, the predominant component of intensity $1-p$ being polarized in the plane of the storage ring. We denote by k the ratio of the intensity of x rays scattered through a given angle θ in the plane of the storage ring ($\phi=0$) to the intensity scattered through the same angle θ in a plane perpendicular to that of the storage ring ($\phi=90°$). Then the fraction of the incident beam that is polarized in the storage-ring plane ($\phi=0$) is

$$1-p = 1 - \left[\frac{k-\cos^2\theta}{(1+k)\ \sin^2\theta} \right] . \tag{4}$$

The range of the azimuthal angle ϕ across the detector window introduced a variation in the cross section that never exceeded 5×10^{-3}.

Scattered intensities were measured at $\phi=0°$ and $\phi=90°$ in all cases where physical constraints permitted; in circumstances where only one angle ϕ was accessible, the measurements were repeated with the same photon energy

at the same azimuthal angle and a different scattering angle θ. Typical observed beam polarizations under various operating conditions are listed in Table I.

The expected polarization of the synchrotron radiation beam is easily calculated from formulas given by Jackson.[18] The observed polarization is less than that predicted by theory for a perfectly aligned beam. Photons from a source of 0.16-cm height (full-width at half-maximum),[14] passing through a 0.1-cm high collimating slit 20 m from the source, should theoretically be ~98 percent polarized in the plane of the storage ring, before Bragg reflections by the monochromator crystal. The monochromator will further increase the degree of polarization. In practice, it is conceivable that the position of the electron beam in the source region of the storage ring (held steady to ±0.02 cm through a feedback control system) may have been slightly off the median plane of the ring during some runs. In particular, greater instabilities occur in the beam at lower electron energies. The beam is positioned by visual observation (through closed-circuit television) of an image on a fluorescent screen. This image is produced by ultraviolet radiation, hence it is much larger than the cross section of the x-ray beam. If the electron beam in the source region were as much as 0.1 cm off the median plane of the ring, the theoretical polarization would decrease from ~98 percent (as indicated above) to ~93 percent in the plane of the ring. Clearly, an experimental determination of beam polarization is important in each experiment in which this property is relevant.

B.   Relative Scattering Cross Sections

X rays can be scattered into the detector from any point along a path that is nearly 10 cm long (Fig. 4). Both the solid angle subtended by the detector and the scattering angle θ depend upon the position z along the beam axis from which a photon is scattered. The total number of photons scattered into the detector can be expressed as

$$N = N_0 \; \rho \int_{-\infty}^{\infty} e^{-\mu z} I\left(\theta(z),\phi\right) \; \Omega(z) dz, \tag{5}$$

where I is the differential cross section per atom (or molecule), N_0 is the number of incident photons, ρ is the number density of gas atoms (or molecules), Ω is the solid angle subtended by the detector, and the factor $e^{-\mu z}$ takes account of the attenuation of the beam along its path.

Because the photoelectric and scattering cross sections for He and H_2 are extremely small, the attenuation factor $e^{-\mu z}$ can be ignored here. Even in the worst situation (for 6-keV photons on He), the attenuation across the scattering region is <0.02 percent. Thus, multiple scattering is negligible: the probability that a photon enters the detector after double scattering is 10^{-7} times less than for single scattering.

The best method to compute experimental differential cross sections, it was found, was to compare the measured scattered intensities with theoretical intensities computed according to Eq. (5) on the basis of suitable theoretical cross sections. The path z was divided into a number of short segments. Solid angles were determined analytically at the center of each segment, from the geometry of the chamber. With theoretical differential cross sections also evaluated at the center of each segment,

the integration in Eq. (5) was performed numerically. In this manner,
theoretical scattering probabilities $N(S)/N_0$ were calculated, as a function
of the parameter $S=(4\pi/\lambda)\sin(\theta/2)$.

We choose a reference value S_0 of the variable S at which the relative
experimental cross sections are to be normalized to theoretical cross
sections. The normalization point S_0 is chosen at high momentum transfer,
where the detailed nature of the H_2 and He wave functions does not influence
the theoretical scattering cross sections, as these closely approach their
asymptotic limit equal to the Klein-Nishina cross section times the number
of electrons. Thus, we take $S_0=6.55$ Å^{-1} for H_2 and $S_0=11.24$ Å^{-1} for He.

The experimental differential scattering cross section at a point S,
relative (i.e., normalized) to the theoretical cross section at S_0, is then
found in the following manner. We take the ratio of scattered-photon
intensities per unit flux at S and S_0 and divide by the ratio of theoretically
predicted scattered intensities at S and S_0, computed as described above.
This predicted ratio includes the effect of the Breit-Dirac recoil factor,
solid angle as a function of scattering angle, and averaging over the small
range of S covered by each measurement. We then multiply by the theoretical
differential cross section at S:

$$\frac{d\sigma(S)}{d\Omega}\bigg|_{\substack{\text{exp.} \\ \text{relative to } S_0}} = \frac{\left[\dfrac{N(S)/N_0}{N(S_0)/N_0}\right]_{\text{exp.}}}{\left[\dfrac{N(S)/N_0}{N(S_0)/N_0}\right]_{\text{theo.}}} \quad \frac{d\sigma(S)}{d\Omega}\bigg|_{\text{theo.}} \quad (6)$$

In Table II, the measured relative total photon scattering cross sections of He are listed, compared with Brown's[11] theoretical cross sections. These theoretical He cross sections were calculated according to the Waller-Hartree theory[3] from 120-term configuration-interaction wave functions, which lead to ground-state energies that agree with the most accurate data to ±0.02 percent. The Brown cross sections agree with the results from Hylleraas-type wavefunctions to within 4 significant figures.

The experimental relative scattering cross sections of H_2 are listed in Table III. Comparison is made with theoretical cross sections computed by Bentley and Stewart.[8] The Bentley-Stewart cross sections were calculated from a natural-orbital expansion of the Kolos-Roothaan H_2 wave functions. These wave functions probably give the best description of the hydrogen molecule. The cross sections were calculated according to the Waller-Hartree theory.[3] Evaluation of the scattering calculations by means of the Tavard sum rule[4] indicates consistency with the initial wave functions to 5 decimal places.[3]

Uncertainties in the measured relative cross sections are small because the method of normalization minimizes the effect of errors in chamber geometry, alignment, and beam polarization. Scattered-photon statistics were excellent due to the intense flux available from the synchrotron source. The main uncertainties in the relative results originate from errors in scattering-chamber dimensions (~0.7 percent) and from the statistical uncertainty in the ratios of scattered intensities (0.7 to 1.5 percent).

C. Absolute Cross Sections

Absolute total photon scattering cross sections were determined by taking measured scattered intensities per unit flux, dividing these by theoretical intensities per unit flux calculated according to Eq. (5), and multiplying by theoretical cross sections:

$$\frac{d\sigma(S)}{d\Omega}\bigg|_{exp.} = \frac{[N(S)/N_0]_{exp.}}{[N(S)/N_0]_{theo.}} \frac{d\sigma(S)}{d\Omega}\bigg|_{theo.} \qquad (7)$$

Theoretical intensities included corrections for temperature and pressure variation, beam width, and differential window absorption. Because the absolute measurements needed to be performed at much lower incident-beam intensities than the relative measurements, only scattering at azimuthal angles $\phi=90°$ could be determined. A direct measurement of the incident-beam polarization was therefore not possible. For the purpose of determining the absolute cross sections, it was assumed that the incident-beam polarization during these runs was the same as observed in the relative scattering runs, i.e., 96 to 97 percent in the storage ring plane ($\phi=0$ deg) (Table I). This assumption is uncertain, as discussed in Sec III.A. Relative scattering measurements were made with a stored-electron energy near 3 GeV, while the lower flux needed for absolute scattering measurements arose from runs at different times, with stored-electron energies closer to 2 GeV. A 2-percent deviation from the assumed beam polarization will cause a ~1-percent error in the absolute measurements. Furthermore, the absolute measurements are much more sensitive than relative measurements to uncertainties in chamber alignment, gas density, and attenuation coefficients, and require the difficult calibration of photon flux in terms of ionization-chamber current

(Sec. II.B.5). Estimated errors in the measured absolute cross sections
are listed in Table IV; the assigned total uncertainty is greatly increased
by the effect of a possible variation in incident-beam polarization.
Measured absolute photon scattering cross sections of He and H_2 are listed
in Table V.

D. Discussion

The measured absolute photon scattering cross sections of both He
and H_2 agree with theory (Table V) within the relatively large probable
errors (Table IV) that are mostly due to possible variations in beam
polarization (Sec. III.A). These uncertainties do not affect the _ratios_
of the measured absolute cross sections of He to those of H_2, and these
ratios, for any given value of S, agree to one percent or better with
theoretical He-to-H_2 cross-section ratios computed with correlated wave
functions.

The measured relative total differential photon scattering cross
sections agree remarkably well with theoretical results that take electron-
electron Coulomb correlation into account [8,10] (Figs. 9 and 10). The effect
of correlation is, in fact, strikingly reflected in the H_2 cross sections,
as shown in Fig. 10 where we have also plotted theoretical cross sections
derived from independent-particle Hartree-Fock wave functions.

The present results suggest that total photon scattering from low-Z
systems can indeed serve as a sensitive test of wave functions and may yield
Coulomb correlation energies, as proposed by Bentley and Stewart.[9]

ACKNOWLEDGMENTS

[1] W. J. Veigele, E. Brigg, L. Bates, E. M. Henry, and B. Bracewell, Kaman Sciences Corporation Report No. DNA 2433F (Formerly DASA 2433), Vol. 1 Revision 1 KN-71-431(R), 1971 (unpublished).

[2] L. S. Bartell and R. M. Gavin, Jr., J. Am. Chem. Soc. 86, 3493 (1964).

[3] I. Waller and D. R. Hartree, Proc. Roy. Sec. A124, 119 (1929).

[4] C. Tavard and M. Roux, C. R. Acad. Sci. (Paris) 260, 4933 (1965).

[5] B. Crasemann, P. E. Koblas, T.-C. Wang, H. E. Birdseye, and M. H. Chen, Phys. Rev. A 9, 1143 (1974).

[6] S. K. Ride and A. B. C. Walker, Astrophys. J. 212, 0000 (1977).

[7] E. O. Wollan, Phys. Rev. 37, 862 (1931).

[8] R. W. Aman, Ph.D. thesis, University of Oregon, 1971 (unpublished).

[9] J. J. Bentley and R. F. Stewart, J. Chem. Phys. 62, 875 (1975).

[10] C. Carter, N. H. March, and D. Vincent, Proc. Phys. Soc. 71, 2 (1958).

[11] R. T. Brown, EG+G Report No. EGG-1183-1453, L-958, 1969 (unpublished).

[12] A. D. Baer, R. Gaxiola, A. Golde, F. Johnson, B. Salsburg, H. Winick, M. Baldwin, N. Dean, J. Harris, E. Hoyt, B. Humphrey, J. Jurrow, R. Melen, J. Miljian, and G. Warren, IEEE Trans. NS-22, 1794 (1975).

[13] B. M. Kincaid, Stanford Synchrotron Radiation Project Report No. 75/03, 1975 (unpublished).

[14] H. Winick and I. Lindau, in Proceedings, ERDA X- and Gamma-Ray Symposium, Ann Arbor, Michigan, ERDA Report No. CONF-760593, 1976 (unpublished).

[15] The scattering chamber was constructed in the shops of the Lawrence Livermore Laboratory.

[16] J. R. Young, Rev. Sci. Instr. __34__, 891 (1963).

[17] D. R. Chipman, Acta Cryst. __A25__, 209 (1969).

[18] J. D. Jackson, _Classical Electrodynamics_ (Wiley, New York, 1975), p. 674.

TABLE I. Measured fraction, 1-p, of the synchrotron radiation beam that is polarized in the plane of the electron accelerator ring.

Scatterer	$h\nu$(keV)	1-p
He	6	0.96(1)
	12	0.98(1)
H_2	5	0.96(1)
	6	0.97(1)
	7	0.96(1)

TABLE II.   Experimental relative total photon scattering cross sections of He.[a]

θ(deg)	$h\nu$(keV)	S (Å^{-1})	$\dfrac{(d\sigma/d\Omega)_{exp.}}{(d\sigma/d\Omega)_{theo.}}$	$\dfrac{(d\sigma/d\Omega)_{exp.}}{(d\sigma/d\Omega)_{Thomson}}$
60.9	6.00	3.04	1.001	2.73 (7)
135.6	6.00	5.61	0.987	2.10 (4)
60.9	12.00	6.08	0.987	2.06 (4)
135.6	12.00	11.24	1^b	2.00^b

[a]Comparison is made with theoretical cross sections of Brown (ref. 11).

[b]Normalization point.

TABLE III. Relative total photon scattering cross sections of H_2.[a]

θ(deg)	hν(keV)	S (Å^{-1})	$\dfrac{(d\sigma/d\Omega)_{exp.}}{(d\sigma/d\Omega)_{theo.}}$	$\dfrac{(d\sigma/d\Omega)_{exp.}}{(d\sigma/d\Omega)_{Thomson}}$
60.9	5.00	2.54	0.996	2.39(3)
60.9	6.00	3.04	1.007	2.22(3)
60.9	7.00	3.55	0.986	2.06(3)
135.6	5.00	4.68	1.001	2.00(3)
135.6	6.00	5.62	1.005	2.00(3)
135.6	7.00	6.56	1.000	2.00(3)[b]

[a]Comparison is made with theoretical cross sections of Bentley and Stewart

(ref. 9).

[b]Normalization point.

TABLE IV. Uncertainties in the absolute total photon scattering measurements.

Scattered peak	±1.5 percent
Ion-chamber calibration	±2 percent
Scattering-chamber dimensions	±1 percent
Scattering-chamber alignment	±1 percent
Foil calibration	±0.7 percent
Attenuation in air and Be	±1 percent
X-ray beam polarization	$\left\{\begin{array}{l} +5 \\ -2 \end{array}\right.$ percent
Total uncertainty	$\sim\left\{\begin{array}{l} +7 \\ -5 \end{array}\right.$ percent

TABLE V. Absolute measured total scattering cross sections of He and H_2.[a]

Scatterer	θ (deg)	$h\nu$ (keV)	$\dfrac{(d\sigma/d\Omega)_{exp.}}{(d\sigma/d\Omega)_{theo.}}$	$\dfrac{(d\sigma/d\Omega)_{exp.}}{(d\sigma/d\Omega)_{Thomson}}$
H_2	135.6	6.00	$0.936\binom{+65}{-44}$	$1.87\binom{+12}{-\ 9}$
	60.9	6.00	$0.957\binom{+67}{-45}$	$2.03\binom{+13}{-10}$
	60.9	7.00	$0.950\binom{+67}{-45}$	$1.99\binom{+13}{-10}$
He	135.6	6.00	$0.958\binom{+67}{-45}$	$2.04\binom{+13}{-10}$
	60.9	6.00	$0.952\binom{+67}{-45}$	$2.60\binom{+18}{-13}$

[a]Results are compared with theoretical cross sections of Bentley and Stewart (ref. 9) for H_2 and of Brown (ref. 11) for He, and with the classical Thomson cross section, $(d\sigma/d\Omega)_{Thomson} = 0.0397(1+\cos^2\theta) \times 10^{-24}$ cm^2.

Figure Captions

FIG. 1. Interaction cross sections for 5-keV photons, as a function of target atomic number Z. Inelastic (incoherent) scattering cross sections are seen to be approximately proportional to Z, while elastic (coherent) scattering is more nearly proportional to Z^2, and the photoionization cross sections increase as Z^5 as long as the incident-photon energy exceeds the K-shell binding energy. The data are from the tabulation of Veigele et al. (ref. 1).

FIG. 2. Experimental relative total photon scattering cross sections for He, as measured by Wollan (ref. 7), compared with theoretical cross sections due to Brown (ref. 11). The Breit-Dirac recoil factor has been removed from the experimental data by multiplying them with $\eta^{-1} = [I_{elastic} + (\nu/\nu')^3 I_{inelastic}] I_{total}^{-1}$, and the data points have been normalized to theory in the large-S limit.

FIG. 3. Schematic representation of apparatus.

FIG. 4. Scattering chamber.

FIG. 5. Block diagram of electronics for processing signals from the proportional counter and in-line transmission ion chamber.

FIG. 6. Spectrum of 6-keV photons scattered by He. The smaller peak represents scattered photons from the n=2, 12-keV harmonic in the incident beam.

FIG. 7. Gas flow system.

FIG. 8. The Cu K absorption edge, represented by the ratio of currents from transmission ion chambers placed upstream (I_o) and downstream (I) from a Cu sample.

FIG. 9. Experimental relative total photon scattering cross sections of He, compared with theoretical results of Brown (ref. 11).

FIG. 10. Experimental relative total photon scattering cross sections of H_2 gas, compared with theoretical results of Bentley and Stewart (ref. 9).
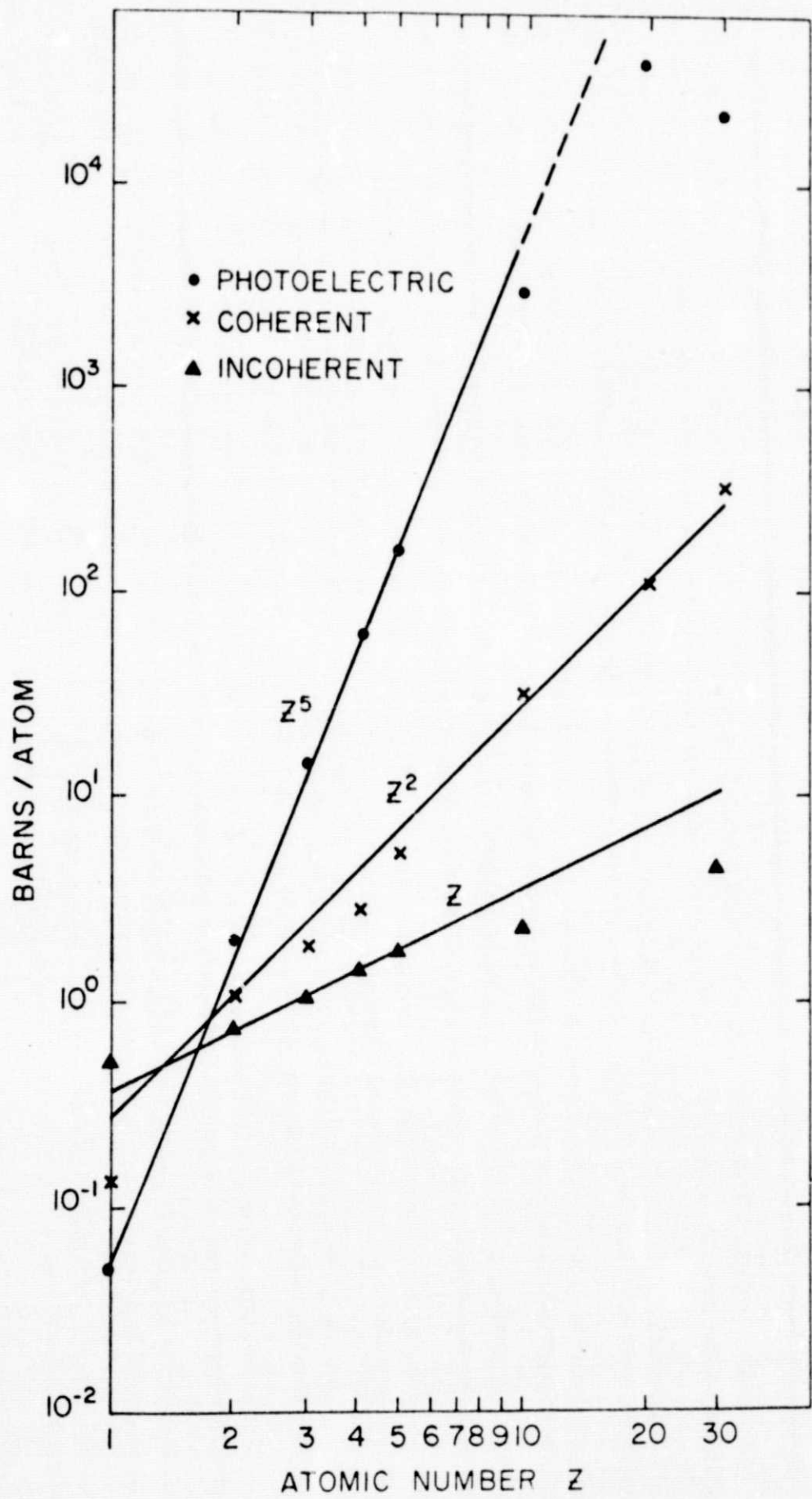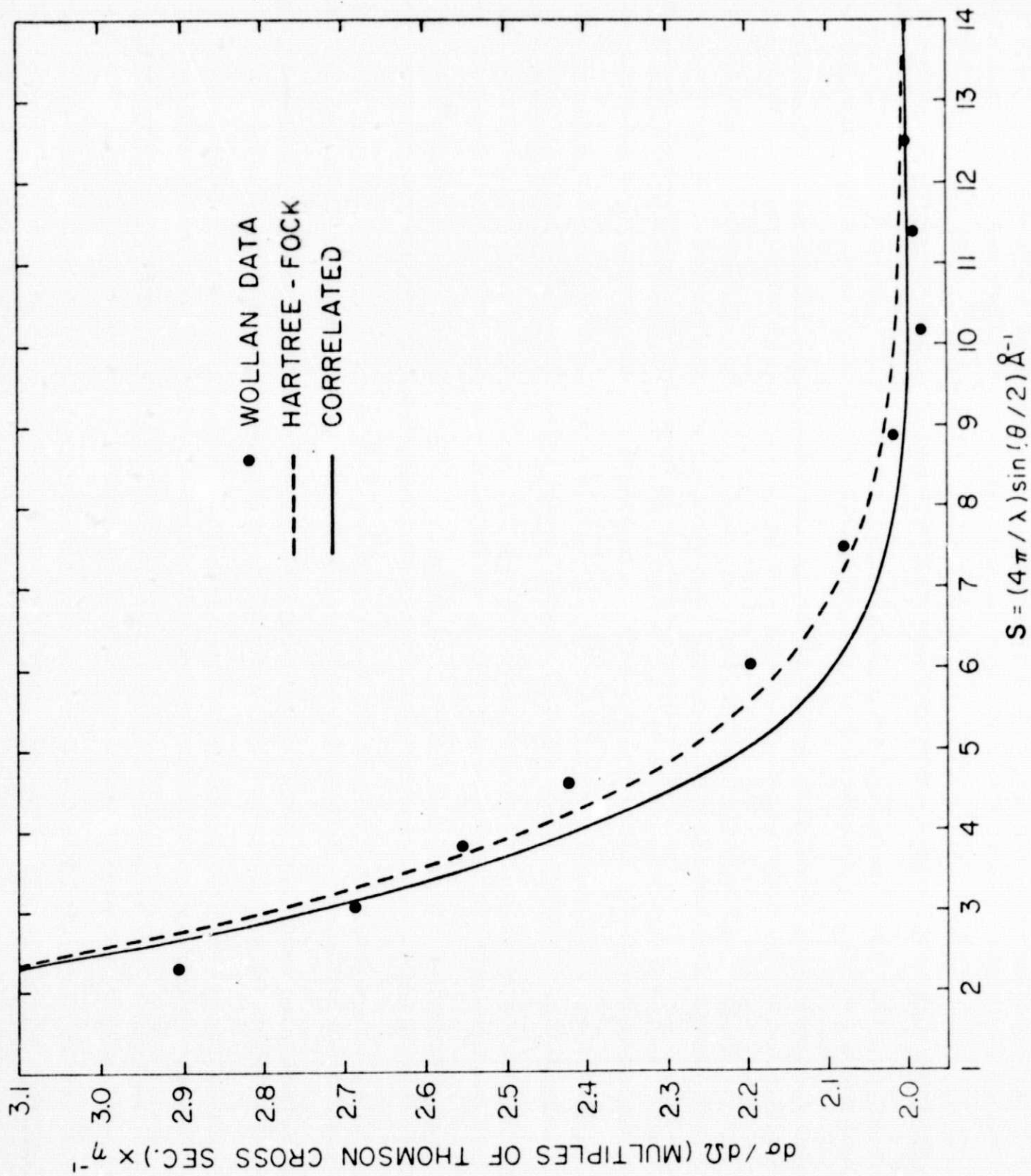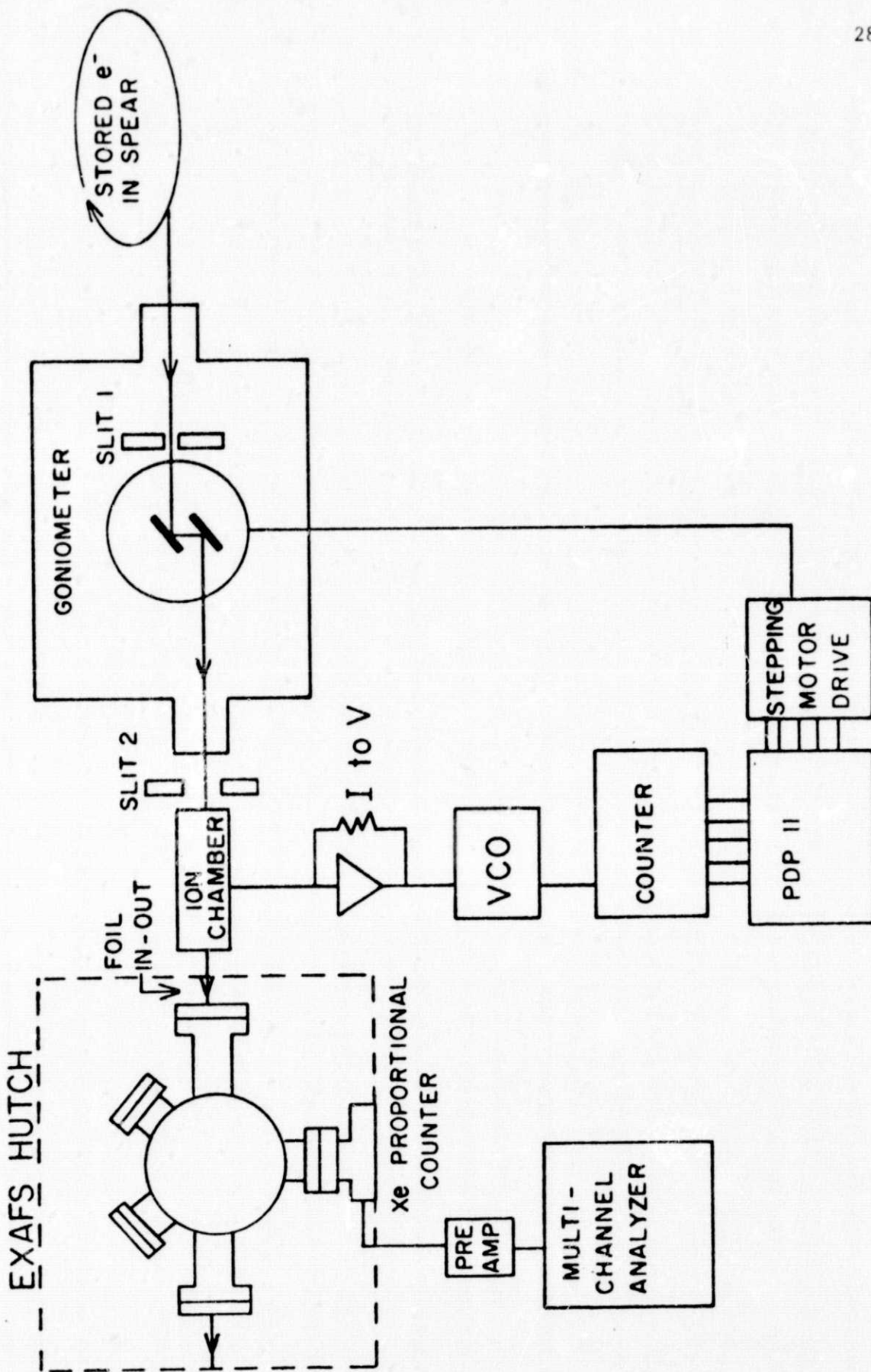
FIG. 1

FIG. 2

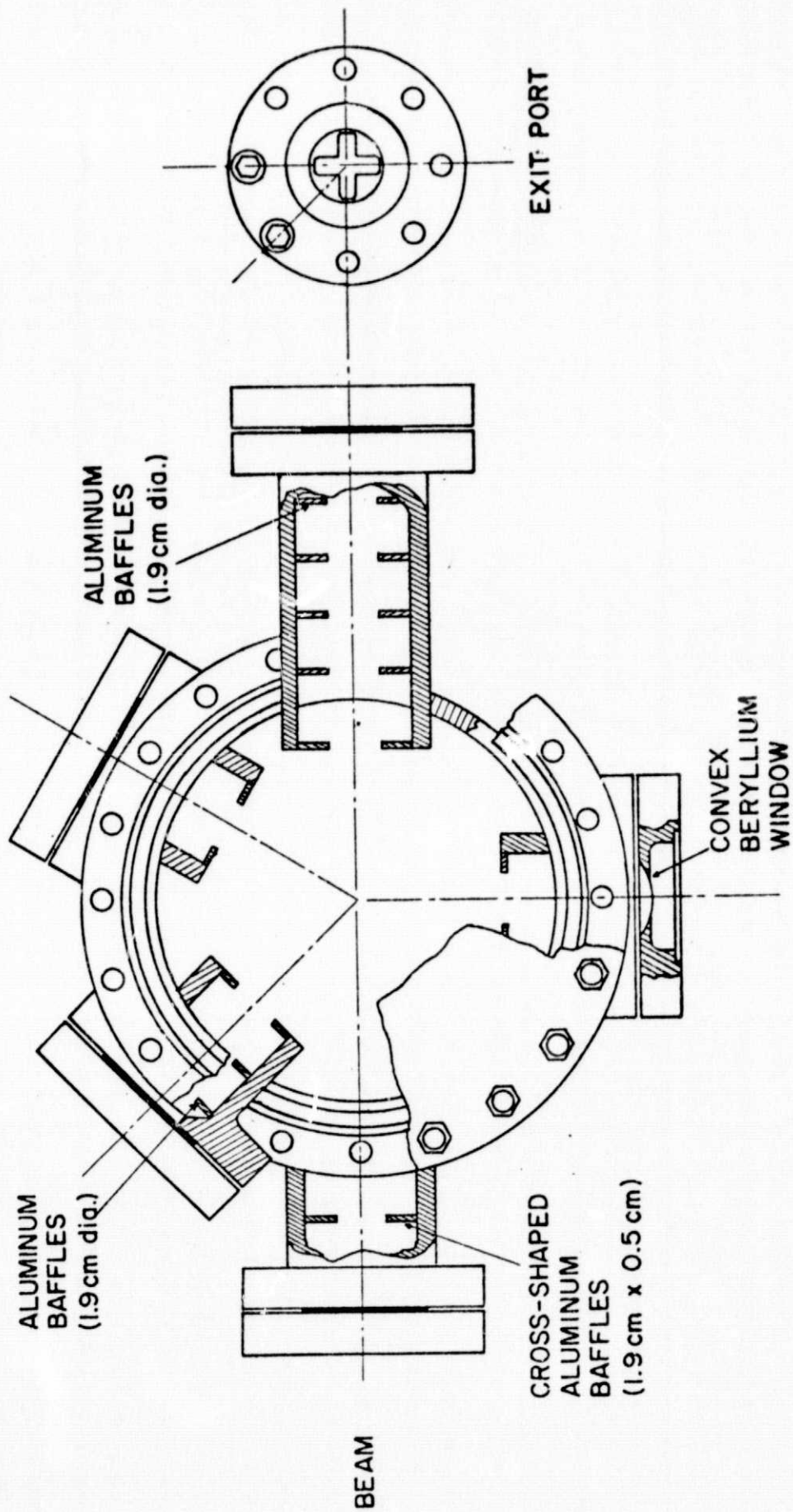$S = (4\pi/\lambda)\sin(\theta/2)\,\text{Å}^{-1}$

• WOLLAN DATA
-- HARTREE - FOCK
— CORRELATED

$d\sigma/d\Omega$ (MULTIPLES OF THOMSON CROSS SEC.) $\times \eta^{-1}$

FIG. 3

ALUMINUM BAFFLES (1.9 cm dia.)

ALUMINUM BAFFLES (1.9 cm dia.)

CONVEX BERYLLIUM WINDOW

CROSS-SHAPED ALUMINUM BAFFLES (1.9 cm x 0.5 cm)

BEAM

EXIT PORT

FIG. 4

FIG. 5

He RUN 28
hν = 6.000 keV
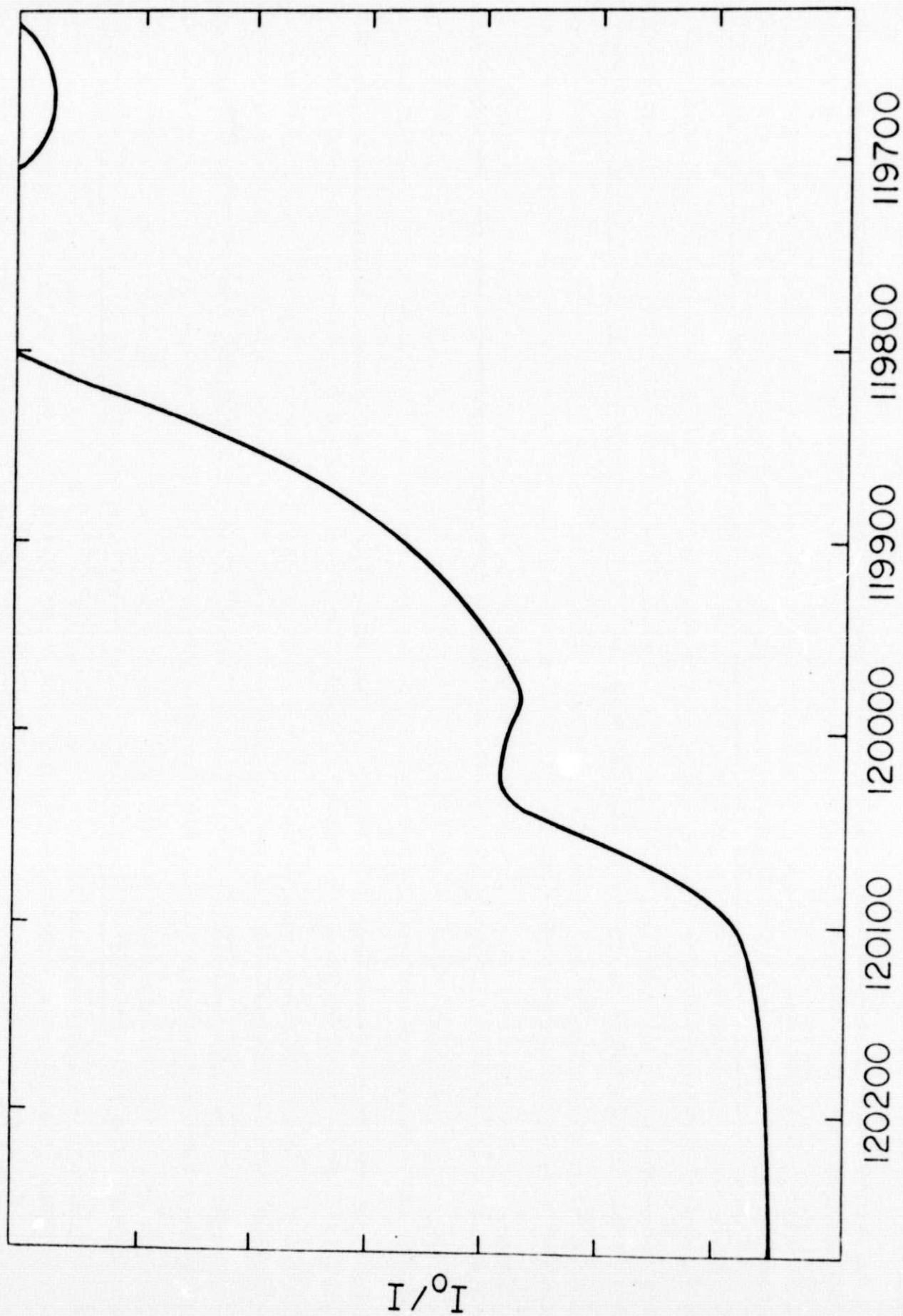θ = 135°
φ = 67°
Ee = 2.96 GeV
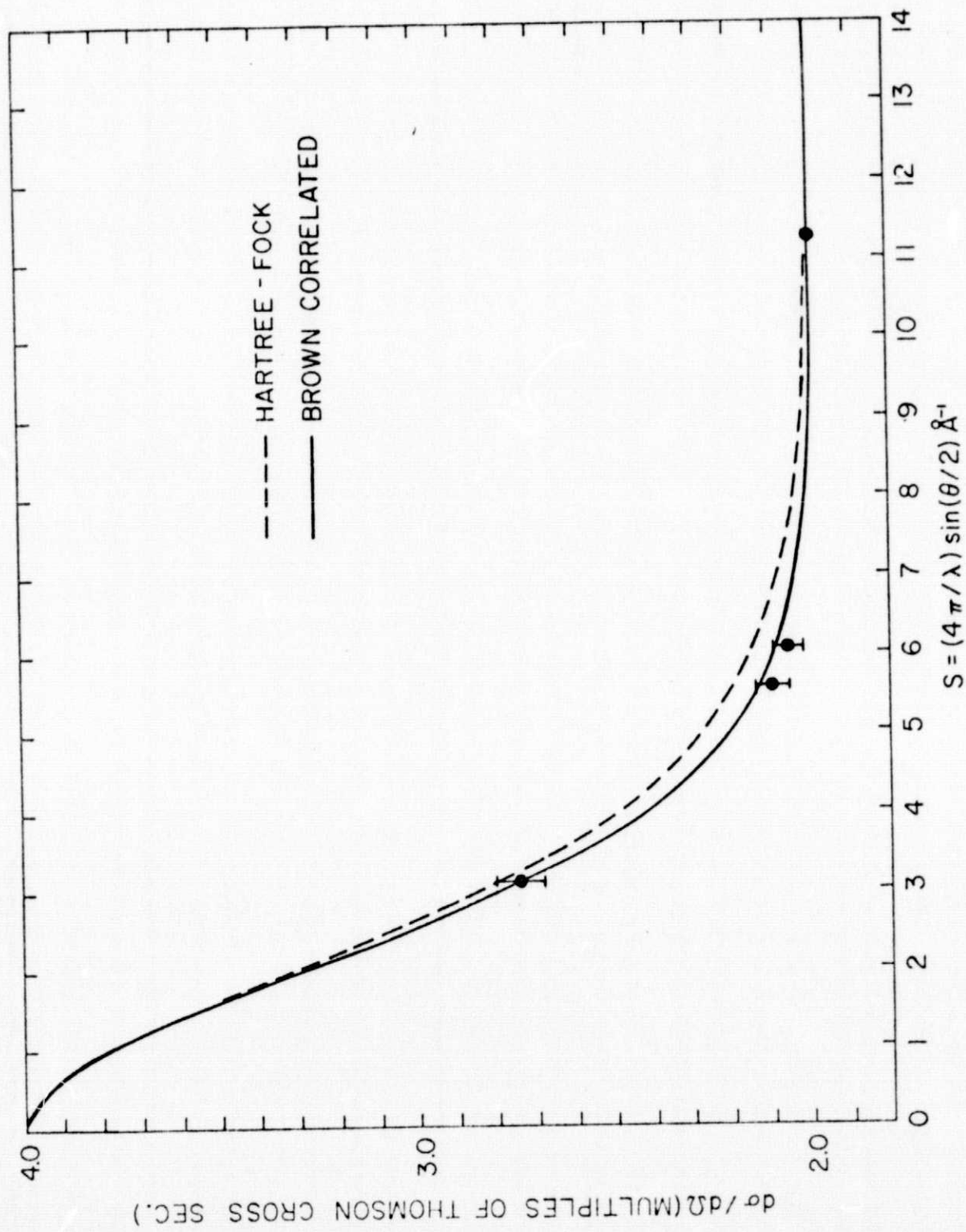1000 sec.

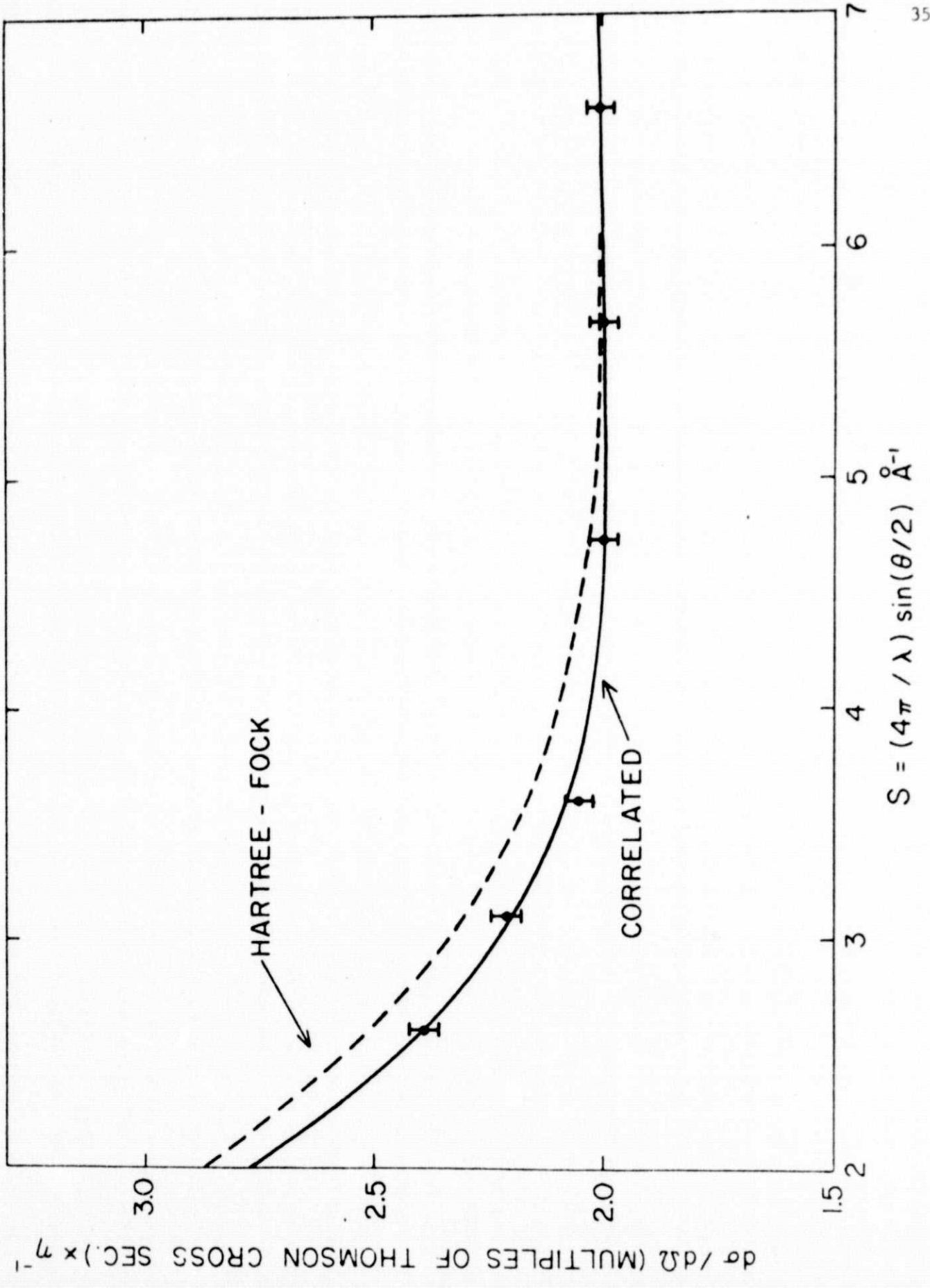CHANNEL NO.

PHOTONS
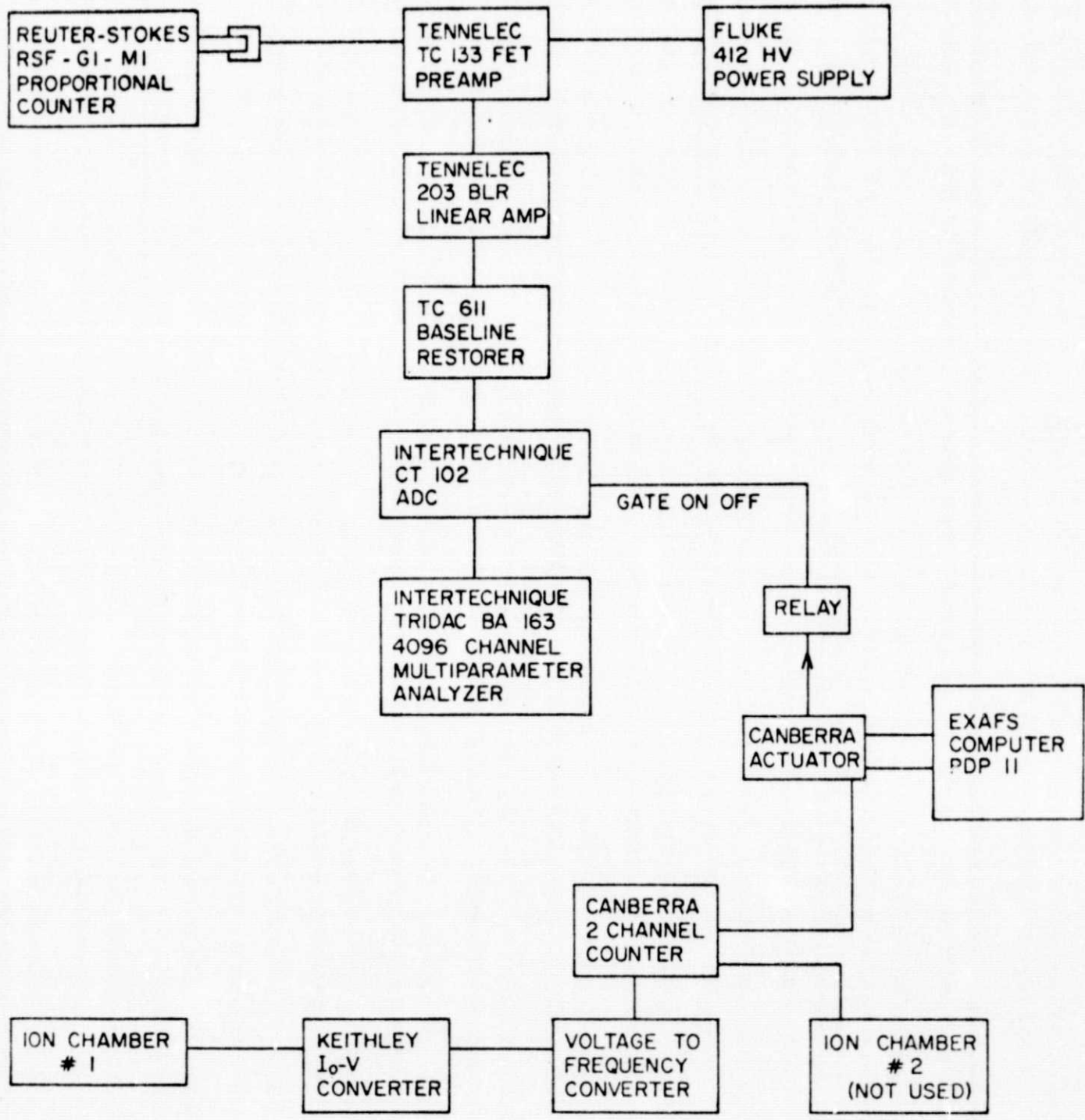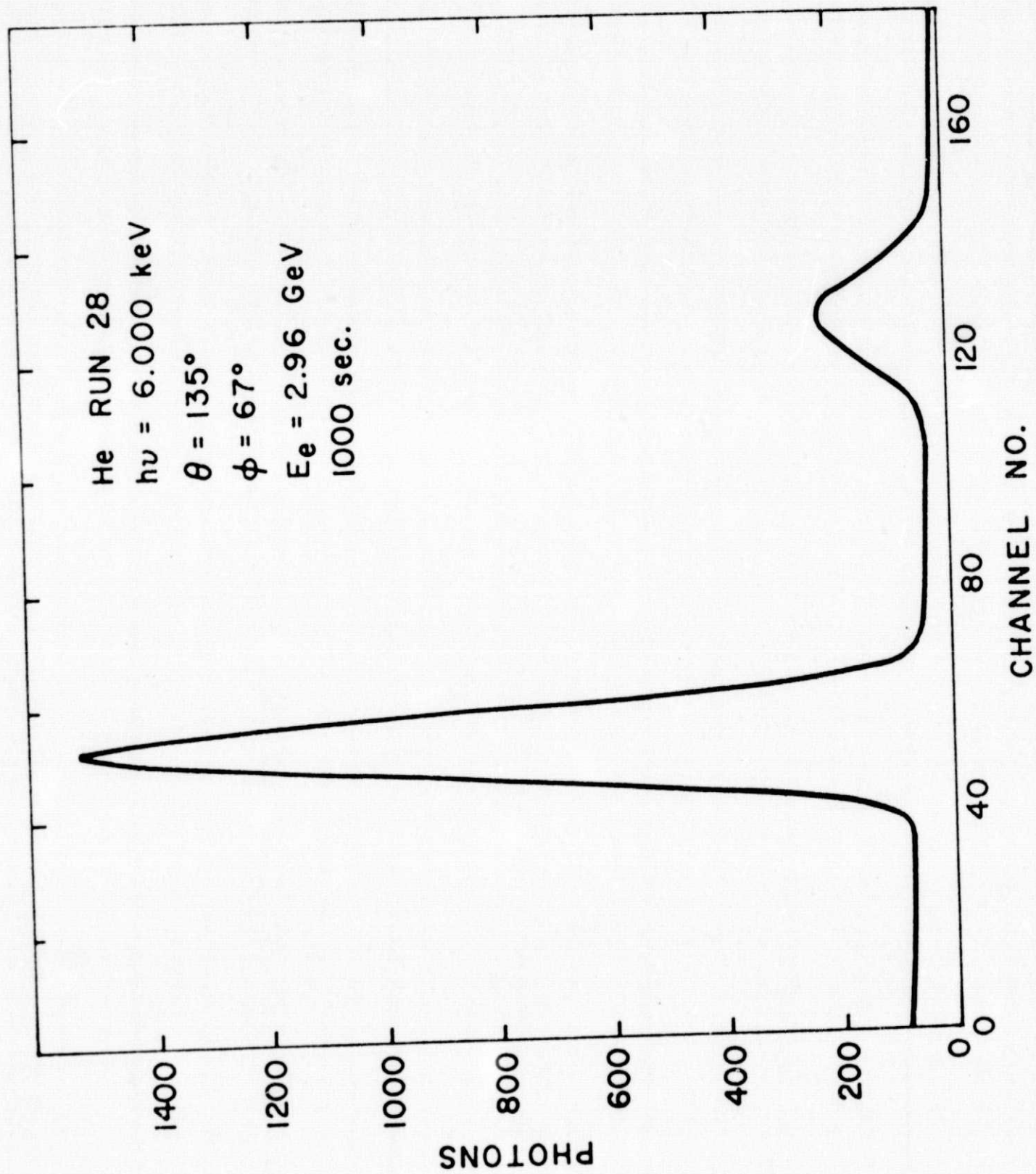
FIG. 6
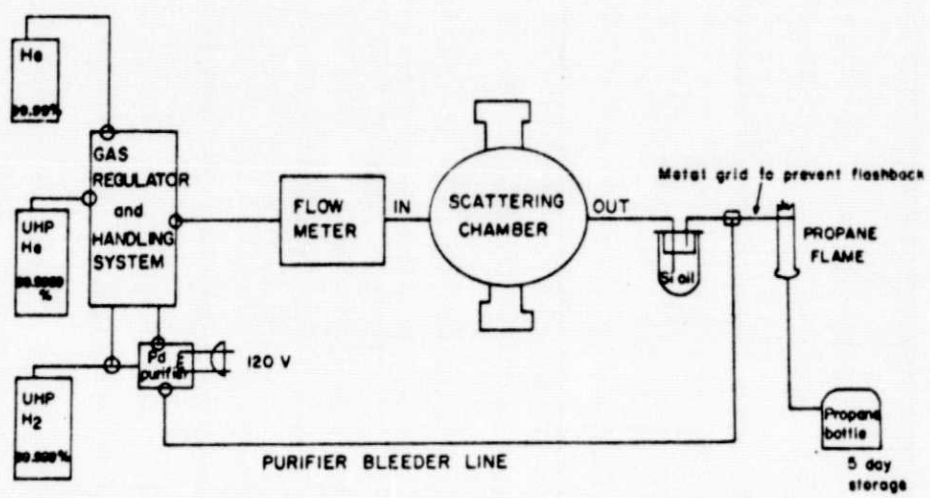
FIG. 7

MONOCHROMATOR STEPPING MOTOR UNITS

FIG. 8

33

FIG. 9

FIG. 10

$S = (4\pi / \lambda) \sin(\theta/2)$ Å^{-1}

$d\sigma/d\Omega$ (MULTIPLES OF THOMSON CROSS SEC.) $\times \eta^{-1}$

HARTREE - FOCK

CORRELATED